actuators

MDPI

Article

Interval Type-2 Fuzzy and Interval Type-2 Fuzzy Sliding-Mode Control for Angular Regulation of a VTOL Plant: An Experimental Study

Steven Nicolalde [1], Luis Morales [1] and David Pozo-Espín [2,*]

[1] Departamento de Automatización Y Control Industrial, Escuela Politécnica Nacional, Quito 170525, Ecuador; steven.nicolalde@epn.edu.ec (S.N.); luis.moralesec@epn.edu.ec (L.M.)
[2] Ingeniería en Electrónica y Automatización, Facultad de Ingeniería y Ciencias Aplicadas, Universidad de Las Américas, Quito 170124, Ecuador
* Correspondence: david.pozo@udla.edu.ec

Abstract

This work presents the design and experimental validation of two interval type-2 fuzzy controllers for the angular regulation of a one-degree-of-freedom QNET VTOL plant: a fuzzy controller with a PD+I structure (IT2FL) and a hybrid fuzzy sliding-mode controller (IT2FL-SMC). Both run in a cascade scheme, with the outer loop handling angular position and an inner loop handling motor current. In the IT2FL-SMC, the discontinuous switching term of a conventional sliding-mode controller is replaced by an interval type-2 fuzzy reaching action, while the continuous term is derived from a second-order model of the plant identified experimentally. The footprint of uncertainty is tuned on the platform, and both controllers are compared against PID, conventional SMC, type-1 fuzzy, and type-1 fuzzy sliding-mode controllers under the same conditions. The tests include step-reference changes and physical eccentric-load disturbances applied in both directions. In reference tracking, the IT2FL gives the smoothest actuation, with the lowest total variation of the control input and the shortest settling time. Under both disturbances, the IT2FL-SMC gives the lowest integral absolute and squared errors, though with a more active control signal. The two controllers turn out to be complementary: one favors smooth actuation, the other favors disturbance rejection.

Keywords: interval Type-2 fuzzy logic; sliding-mode control; VTOL; disturbance rejection; control effort; experimental validation

Check for updates

Academic Editor: Liang Sun

Received: 19 August 2026
Revised: 11 September 2026
Accepted: 15 September 2026
Published: 15 October 2026

Copyright: © 2026 by the authors. Licensee MDPI, Basel, Switzerland. This article is an open access article distributed under the terms and conditions of the Creative Commons Attribution (CC BY) license.

1. Introduction

Unmanned aerial vehicles with vertical takeoff and landing capabilities have attracted considerable research attention in recent years. Their use extends well beyond laboratory experiments or academic and military demonstrations—today they are actively deployed in precision agriculture, power-line inspection, package delivery, search-and-rescue operations, and terrain assessment, among other demanding applications [1,2]. A persistent challenge, however, is ensuring that these systems continue to behave reliably when real operating conditions deviate from those assumed during the design phase. Wind disturbances, load variations, motor wear, and unmodeled dynamics are all factors that can compromise controller performance in practice [3,4].

The Quanser QNET VTOL has been widely used as an experimental platform for developing and benchmarking control strategies applicable to aerial vehicles under repro-

ducible conditions [5–7]. The plant consists of an articulated arm with a motor–propeller assembly at one end and a counterweight at the other, with the objective of maintaining a desired pitch angle. Despite its apparent simplicity, the system exhibits nonlinear behavior due to the interaction between the inner current loop, the outer position-control loop, and the aerodynamic forces that vary with rotor speed [8].

Sliding-mode control (SMC) has been one of the most extensively studied strategies for systems with these characteristics, given its well-known robustness against parametric uncertainty and external disturbances [9]. Prior work on this platform has consistently shown that SMC outperforms classical controllers such as PID when the system is subjected to perturbations [5,6]. Two relevant examples are the ISMC-LQI controller proposed by Aguas et al. [5] and the SMC-LQI design reported by Herrera et al. [6], both implemented and experimentally validated on this platform.

The main limitation of conventional SMC is chattering—high-frequency oscillations inherent to the discontinuous switching action that can cause actuator wear, excite unmodeled dynamics, and degrade overall system performance [9,10]. In the Quanser VTOL, these oscillations directly affect the motor's electrical dynamics, which in turn introduces disturbances into the angular-position control of the arm [8]. One common approach to attenuate chattering is to replace the sign function with a smooth approximation, such as a hyperbolic-tangent saturation. This reduces the oscillations but introduces a boundary layer around the sliding surface in which invariance is no longer guaranteed, thereby reducing robustness [10]. More recent work has explored reinforcement learning as a means of reducing chattering in UAV applications, with promising results, although adequate behavior outside the training conditions is not necessarily guaranteed [11].

Higher-order sliding-mode algorithms are another way to reduce chattering, since they move the discontinuous term to a higher derivative of the sliding variable. Super-twisting controllers with adaptive gains have performed well in electric-drive applications. For permanent-magnet motor drives, a barrier-function-based adaptive super-twisting controller tunes its gain online without a known disturbance bound and keeps the tracking error inside a predefined region [12]. A related design combines a super-twisting extended state observer with a quasi-proportional-resonant controller to reject time-varying disturbances that a linear observer cannot handle because of its limited bandwidth [13]. These methods rely on observers and gain adaptation; the approach used here instead replaces the switching term with an interval type-2 fuzzy reaching action.

Fuzzy logic offers a structurally different path to chattering reduction. The approach consists of replacing the switching term of the SMC with a fuzzy inference system, and it has been extensively explored over the past two decades. Most of these proposals, however, rely on Type-1 fuzzy systems, which require membership functions with precisely fixed values. This requirement conflicts with the original motivation of handling uncertainty because the designer is forced to work with specific numerical values, and any error in them has no internal compensation mechanism [14]. Type-2 fuzzy systems address this limitation by making the membership grades themselves uncertain, resulting in a footprint of uncertainty bounded by upper and lower membership functions [15,16]. Consequently, interval Type-2 fuzzy logic controllers (IT2-FLCs) have been shown to outperform their Type-1 counterparts when the degree of system uncertainty is high, a finding validated across robotics, process control, and aerial-vehicle applications [17]. Among the Type-reduction methods reported in the literature, the Karnik–Mendel algorithm is one of the most widely adopted [18].

Interval Type-2 fuzzy logic has been successfully applied to aeronautical-control problems. Sarabakha et al. [19] demonstrated through real quadrotor flights that an IT2 fuzzy PID controller maintains reference tracking under strong wind conditions in which

both classical PID and Type-1 fuzzy controllers exhibit significant performance degradation. Zeghlache et al. [20] designed an interval Type-2 fuzzy sliding-mode controller (IT2FSMC) for a three-degree-of-freedom laboratory helicopter, using the fuzzy system to generate the switching term and proving closed-loop stability through Lyapunov analysis. The same group later extended this result to a fault-tolerant control scenario on a similar platform [21], further strengthening the case for this approach in laboratory aeronautical systems. None of these works, however, addresses the specific configuration considered in this paper: an interval Type-2 fuzzy logic system acting on the sliding surface of an SMC whose equivalent control term is derived from a first-order-plus-dead-time (FOPDT) model identified experimentally on a one-degree-of-freedom Quanser VTOL. To the authors' knowledge, this combination has not been previously reported in the literature. The field is also advancing toward Type-3 fuzzy architectures for UAVs [22], which makes it worthwhile to first establish a solid Type-2 baseline before introducing that additional layer of complexity.

This paper presents the design and experimental validation of an interval Type-2 fuzzy logic sliding-mode controller (IT2FL-SMC) for the one-degree-of-freedom Quanser VTOL system. The control law combines a continuous equivalent term derived from an FOPDT model identified using the reaction-curve method [10] with an interval Type-2 fuzzy term acting on the sliding surface and its derivative. The main contributions of this work are: (i) a systematic design procedure that links the experimentally identified second-order model of the QNET VTOL with the synthesis of an interval Type-2 fuzzy reaching term for the SMC; (ii) experimental evidence that this interval Type-2 fuzzy reaching action improves disturbance rejection at the cost of increased control-input variation; and (iii) a quantitative comparison against PID, conventional SMC, Type-1 fuzzy, and Type-1 fuzzy sliding-mode controllers on the same platform using multiple performance metrics.

The remainder of this paper is organized as follows. Section 2 presents the plant model and the design of the IT2FL and IT2FL-SMC controllers. Section 3 reports the experimental results and comparative discussion. Finally, Section 4 summarizes the main conclusions.

2. Materials and Methods

This section presents the formulation of the proposed control strategies for angular-position regulation of the QNET VTOL plant. The study considers two approaches based on interval Type-2 fuzzy logic: an IT2FL controller with a PD+I structure and a hybrid IT2FL-SMC controller. The first controller is intended to improve the adaptability of the system under uncertainties associated with the plant dynamics, whereas the second integrates the robustness of sliding-mode control with an interval Type-2 fuzzy action designed to smooth the reaching component.

Unlike a conventional Type-1 fuzzy formulation, the IT2FL approach incorporates a footprint of uncertainty in the membership functions, which allows variations in the linguistic information used by the controller to be represented. In the IT2FL-SMC case, this feature is used to replace the typical discontinuous action of conventional SMC with a smoothed fuzzy signal while preserving the reaching criterion of the sliding surface.

2.1. Dynamic Model of the QNET VTOL Plant

The QNET VTOL plant is a one-degree-of-freedom aerodynamic system composed of a rigid arm that rotates about a fixed axis. At one end of the arm, a propulsion unit generates the thrust required to modify the angular position, whereas a counterweight located at the opposite end contributes to the dynamic balance of the system.

The experimental platform used in this work is the Quanser QNET VTOL system, shown in Figure 1. The setup consists of a single-degree-of-freedom rotating arm equipped

with a motor–propeller assembly and a counterweight mechanism. The angular position of the arm is measured by the integrated position sensor, while the propulsion system provides the control action required to regulate the pitch angle. The platform is operated through a real-time control interface, allowing the different control strategies considered in this study to be implemented and evaluated under the same experimental conditions.



Figure 1. Experimental QNET VTOL platform used for controller implementation and validation.

Due to this configuration, the angular response of the VTOL depends on the torque generated by the propeller, the gravitational torques associated with the mass distribution, mechanical friction, and the equivalent inertia of the system [23].

From the torque balance around the rotation axis, the system dynamics can be described by a linear second-order model around the equilibrium point. Under this operating condition, the angular dynamics are expressed as:

$$J\ddot{\theta}(t) + B\dot{\theta}(t) + K\theta(t) = \tau_t(t), \tag{1}$$

where J is the equivalent moment of inertia with respect to the rotation axis, B is the viscous damping coefficient, K is the equivalent stiffness of the system, $\theta(t)$ is the angular position of the arm, and $\tau_t(t)$ is the torque produced by the propulsion system [23].

Considering that the torque generated by the propeller is proportional to the motor current, the following relation is obtained:

$$\tau_t(t) = K_t I_m(t), \tag{2}$$

where K_t is the equivalent thrust or torque constant and $I_m(t)$ is the current applied to the motor. By substituting Equation (2) into Equation (1), the plant dynamics become

$$J\ddot{\theta}(t) + B\dot{\theta}(t) + K\theta(t) = K_t I_m(t). \tag{3}$$

Applying the Laplace transform to Equation (3), assuming zero initial conditions, gives

$$Js^2\Theta(s) + Bs\Theta(s) + K\Theta(s) = K_t I_m(s). \tag{4}$$

Therefore, the transfer function that relates the angular position of the arm to the current applied to the motor is defined as

$$P(s) = \frac{\Theta(s)}{I_m(s)} = \frac{K_t}{Js^2 + Bs + K}. \tag{5}$$

Using the nominal parameters of the QNET VTOL plant, the parameterized transfer function is expressed as

$$G(s) = \frac{0.53}{0.145168s^2 + 0.354519s + 1}. \tag{6}$$

The model in Equation (6) is adopted as the nominal representation for the design of the proposed controllers. This choice is justified because the identified response reproduces the real system behavior more accurately within the experimental operating range. Consequently, the tuning of both the IT2FL and IT2FL-SMC controllers is developed from this model, considering the plant angular position as the controlled variable.

The tracking error is defined as

$$e(t) = r(t) - y(t), \tag{7}$$

where $y(t)$ is the measured angular position and $r(t)$ is the desired reference. The control objective is to make the angular output follow the reference trajectory with reduced error, even under setpoint changes and external disturbances. Hence, the desired condition is

$$\lim_{t\to\infty} e(t) \to 0. \tag{8}$$

2.2. Cascade Control Structure

The controller design is based on a cascade control structure. This choice follows from the dynamic nature of the system, which involves two behaviors with different time scales: the electrical dynamics of the motor, associated with the current, and the mechanical dynamics of the arm, associated with the angular position. If the position is controlled directly using a single outer loop, the controller must compensate for both the actuator response and the angular dynamics of the plant. This may introduce delays and reduce the robustness of the overall system.

In the adopted structure, the inner loop regulates the motor current using a previously tuned PI controller, whereas the outer loop controls the angular position. This separation allows the electrical dynamics to be compensated by the inner loop, so that the outer controller can focus on position regulation. Thus, the signal generated by the outer controller is interpreted as a current reference for the inner loop [23].

Under this configuration, the IT2FL and IT2FL-SMC controllers are designed for the outer position loop. The tuning of the inner loop is kept fixed throughout the tests in order to directly evaluate the performance of the proposed strategies on the angular dynamics of the VTOL.

2.3. IT2FL Controller Design

The proposed IT2FL controller is structured as an interval Type-2 fuzzy system with a PD+I architecture. The main fuzzy action uses the tracking error and its time derivative as input variables, while the integral action is incorporated in parallel to reduce the steady-state error. This configuration combines a fast transient response, associated with the PD-like fuzzy action, with improved steady-state accuracy provided by the integral branch. The controller scheme is shown in Figure 2.

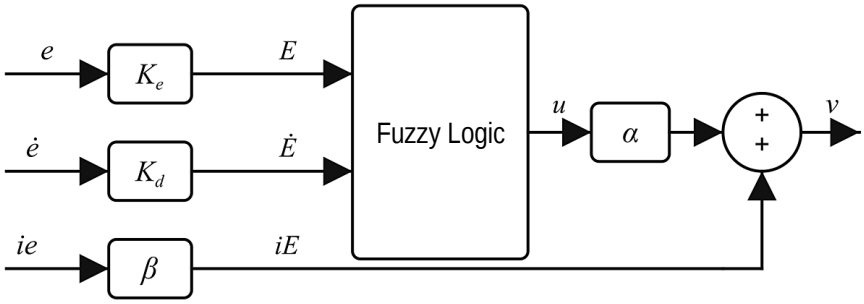


Figure 2. Architecture of the fuzzy PD+I controller.

The control signal generated by the IT2FL controller is defined as

$$v(t) = \alpha u_{\mathrm{IT2}}(t) + \beta \int e(t)\,\mathrm{d}t, \tag{9}$$

where $u_{\mathrm{IT2}}(t)$ is the defuzzified output of the interval Type-2 fuzzy system, α is the scaling gain of the fuzzy action, and β is the gain associated with the integral action. The gain α adjusts the intensity of the fuzzy response, whereas β modifies the integral contribution to reduce the permanent error.

The fuzzy system is implemented as a multiple-input/single-output (MISO) structure, with two input variables and one output variable. The inputs are the error $e(t)$ and its derivative $\dot{e}(t)$, whereas the output is the fuzzy control action $u_{\mathrm{IT2}}(t)$. Before entering the inference system, the inputs are normalized through scaling gains [24]:

$$E(t) = K_e e(t), \tag{10}$$

$$\dot{E}(t) = K_D \dot{e}(t), \tag{11}$$

where K_e and K_D adjust the operating range of the input variables. The normalized variables $E(t)$ and $\dot{E}(t)$ are defined over the universe of discourse $[-1, 1]$, which makes it possible to work with bounded ranges and to separate the tuning of the membership functions from the adjustment of the external controller gains.

Five linguistic labels are used for the fuzzy inputs: NB, NS, Z, PS, and PB, which correspond to Negative Big, Negative Small, Zero, Positive Small, and Positive Big, respectively. Each label is represented by an interval Type-2 triangular membership function. Triangular functions were selected because of their low computational complexity and because preliminary tests showed no significant improvement when using more complex membership functions [25].

In an interval Type-2 fuzzy set, each membership function is defined by an upper membership function (UMF) and a lower membership function (LMF). The region between both functions is known as the footprint of uncertainty (FOU) [24]. In this work, the upper membership function is kept fixed, whereas the lower membership function is modified to adjust the uncertainty width. For an upper triangular membership function defined by the parameters (a, b, c), the lower membership function is parameterized as

$$\mathrm{LMF} = \mathrm{tri}(x; a + \Delta_{\mathrm{FOU}}, b, c - \Delta_{\mathrm{FOU}}), \tag{12}$$

where Δ_{FOU} denotes the width of the footprint of uncertainty. This parameterization keeps the central point of each linguistic set constant and only modifies the limits of the lower function [24]. Thus, the symmetry of the membership functions is preserved while controlling the level of uncertainty included in the controller.

The parameters of the upper membership functions used for the inputs are shown in Table 1.

Table 1. Parameters of the upper triangular membership functions.

Label	Description	Parameters (a, b, c)	Range
NB	Negative Big	$(-1.5, -1.0, -0.5)$	$[-1.5, -0.5]$
NS	Negative Small	$(-1.0, -0.5, 0.0)$	$[-1.0, 0.0]$
Z	Zero	$(-0.5, 0.0, 0.5)$	$[-0.5, 0.5]$
PS	Positive Small	$(0.0, 0.5, 1.0)$	$[0.0, 1.0]$
PB	Positive Big	$(0.5, 1.0, 1.5)$	$[0.5, 1.5]$

As shown in Table 1, although the normalized universe of discourse is limited to the interval $[-1, 1]$, the outermost membership functions, NB and PB, are parameterized up to ± 1.5 to produce shoulder-Type behavior. This allows the maximum membership degree to be maintained at the normalized boundaries and prevents an abrupt decrease in the activation of the rules associated with the outer membership functions. Considering a nominal value of $\Delta_{\text{FOU}} = 0.25$, the lower membership functions are defined as shown in Table 2.

Table 2. Parameters of the lower triangular membership functions for $\Delta_{\text{FOU}} = 0.25$.

Label	Description	Parameters (a, b, c)	Range
NB	Negative Big	$(-1.25, -1.0, -0.75)$	$[-1.25, -0.75]$
NS	Negative Small	$(-0.75, -0.5, -0.25)$	$[-0.75, -0.25]$
Z	Zero	$(-0.25, 0.0, 0.25)$	$[-0.25, 0.25]$
PS	Positive Small	$(0.25, 0.5, 0.75)$	$[0.25, 0.75]$
PB	Positive Big	$(0.75, 1.0, 1.25)$	$[0.75, 1.25]$

The membership functions defined for the IT2FL controller with the selected parameterization are shown in Figure 3.

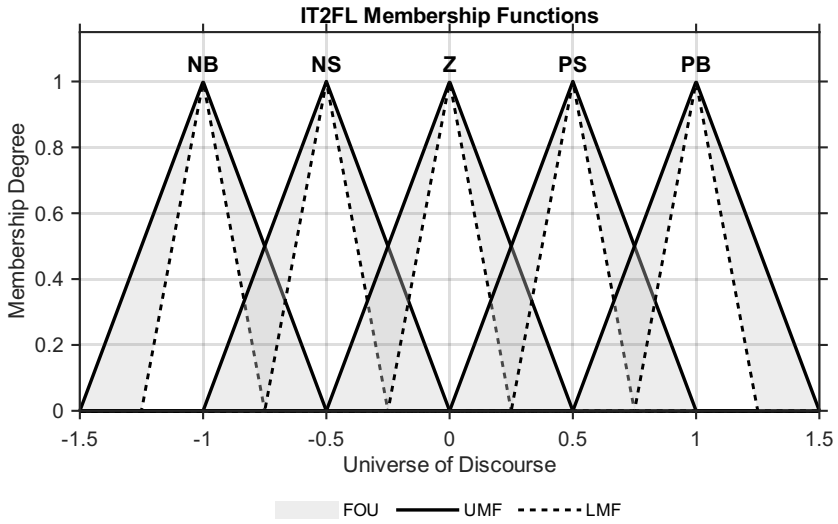


Figure 3. Membership functions defined for the IT2FL controller inputs.

The value of Δ_{FOU} directly affects the controller behavior. A very narrow footprint of uncertainty makes the system response approach that of a Type-1 fuzzy controller, whereas an excessively wide footprint may produce more oscillatory responses due to the increased uncertainty in the inference process [25]. Therefore, the FOU is considered a design parameter that must be experimentally calibrated.

The controller rule base is defined as a 5×5 matrix composed of 25 linguistic rules. The rule structure relates the normalized error and its derivative to the fuzzy control action. The general form of the ith rule is expressed as [25]

$$R_i: \quad \text{If } E(t) \text{ is } A_i \text{ and } \dot{E}(t) \text{ is } B_i, \text{ then } u_{\mathrm{IT2}}(t) \text{ is } C_i. \tag{13}$$

The logical conjunction between antecedents is implemented using the minimum T-norm. Therefore, for each active rule, the lower and upper firing strengths are computed as [25]

$$\underline{f}^{\,i} = \min\left(\underline{\mu}_{A_i}(E), \underline{\mu}_{B_i}(\dot{E})\right), \tag{14}$$

$$\overline{f}^{\,i} = \min\left(\overline{\mu}_{A_i}(E), \overline{\mu}_{B_i}(\dot{E})\right), \tag{15}$$

where $\underline{\mu}$ and $\overline{\mu}$ represent the lower and upper membership grades, respectively. The implemented rule base is shown in Table 3. Its symmetric distribution allows coherent control actions to be generated for both upward and downward reference changes.

Table 3. Rule base of the IT2FL controller.

$\dot{E}(t) \backslash E(t)$	**NB**	**NS**	**Z**	**PS**	**PB**
NB	NB	NB	NB	NS	Z
NS	NB	NB	NS	Z	PS
Z	NB	NS	Z	PS	PB
PS	NS	Z	PS	PB	PB
PB	Z	PS	PB	PB	PB

Interval singleton consequents are used for the controller output. Unlike a Type-1 fuzzy system, where each consequent is represented by a crisp value, the IT2FL system defines each consequent through a lower and an upper bound, as shown in Figure 4.

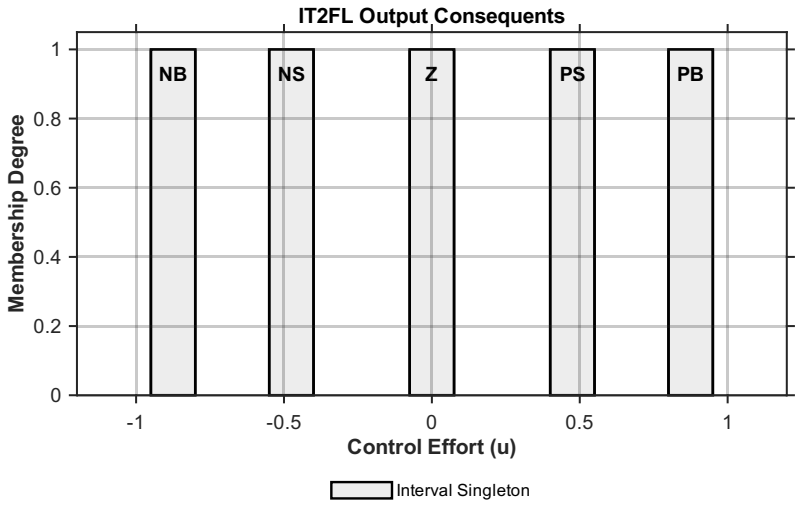


Figure 4. Membership functions defined for the IT2FL controller output.

In the IT2FL controller, the representative value of each consequent is calculated as the midpoint of the interval [18]:

$$y^i = \frac{\underline{y}^{\,i} + \overline{y}^{\,i}}{2}, \tag{16}$$

where $\underline{y}^{\,i}$ and $\overline{y}^{\,i}$ are the lower and upper bounds of the consequent associated with rule i.

Type reduction is performed using the Nie–Tan algorithm because of its lower computational cost compared with iterative methods. This algorithm obtains an equivalent Type-1

output from the lower and upper firing strengths. The defuzzified output is computed as [26]

$$Y_{\mathrm{NT}} = \frac{\sum_{i=1}^{M}\left(\underline{f}^{i} + \overline{f}^{i}\right) y^{i}}{\sum_{i=1}^{M}\left(\underline{f}^{i} + \overline{f}^{i}\right)}, \tag{17}$$

where M denotes the number of active rules at each sampling instant. Although the complete 25-rule base is evaluated during implementation, only the rules with nonzero firing strength effectively contribute to the numerator and denominator of Equation (17). This property reduces the computational burden without modifying the linguistic structure of the controller [26].

The Type-1 fuzzy controller shares the full structure of the IT2FL controller: same scaling gains, same triangular membership functions, same 5×5 rule base, and same singleton consequents. It differs only in having no footprint of uncertainty ($\Delta_{\mathrm{FOU}} = 0$), so its lower and upper membership functions coincide. This is what makes the comparison fair, as any difference in the results comes from the footprint of uncertainty and nothing else.

2.4. IT2FL-SMC Controller Design

The IT2FL-SMC controller is designed from the structure of a conventional sliding-mode controller, but the discontinuous component is replaced by an action generated through an interval Type-2 fuzzy system. With this modification, the continuous component of the SMC preserves its role of compensating the nominal plant dynamics, whereas the fuzzy component provides a smoother reaching action that is robust against uncertainties and disturbances. The implemented IT2FL-SMC scheme is shown in Figure 5.

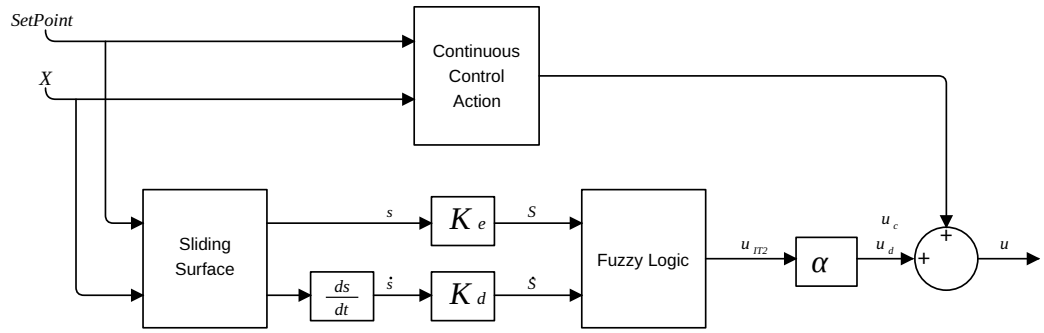


Figure 5. Scheme of the IT2FL-SMC controller.

The total control law is defined as

$$u(t) = u_c(t) + u_d(t), \tag{18}$$

where $u_c(t)$ is the continuous or equivalent component of the controller and $u_d(t)$ is the reaching component.

The continuous component of the sliding-mode controller is obtained through the equivalent-control procedure. The derivation begins with the first-order-plus-dead-time process model:

$$\frac{Y(s)}{U(s)} = \frac{Ke^{-t_0 s}}{\tau s + 1}, \tag{19}$$

where $Y(s)$ is the system output, $U(s)$ is the control signal, K is the process gain, τ is the time constant, and t_0 is the time delay. To obtain a tractable time-domain representation, the delay is approximated using the following first-order rational expression:

$$e^{-t_0 s} \approx \frac{1}{t_0 s + 1}. \tag{20}$$

Substituting Equation (20) into Equation (19) yields

$$\frac{Y(s)}{U(s)} \approx \frac{K}{(\tau s + 1)(t_0 s + 1)}. \tag{21}$$

The model in Equation (21) has a structure similar to that of the transfer function in Equation (6). Expanding the denominator and matching its coefficients with the identified model gives

$$K = 0.53, \qquad t_0\tau = 0.145168, \qquad t_0 + \tau = 0.354519. \tag{22}$$

Therefore,

$$\left[t_0\tau s^2 + (t_0 + \tau)s + 1\right] Y(s) = KU(s). \tag{23}$$

Applying the inverse Laplace transform results in

$$t_0\tau \ddot{Y}(t) + (t_0 + \tau)\dot{Y}(t) + Y(t) = KU(t). \tag{24}$$

Since the approximate model is second order, the sliding surface is defined as

$$S(t) = \frac{\mathrm{d}e(t)}{\mathrm{d}t} + \lambda_1 e(t) + \lambda_0 \int_0^t e(\tau)\,\mathrm{d}\tau. \tag{25}$$

With the tracking error defined in Equation (7), the continuous control component is obtained by imposing the equivalent-control condition

$$\dot{S}(t) = 0. \tag{26}$$

Differentiating the sliding surface gives

$$\ddot{e}(t) + \lambda_1 \dot{e}(t) + \lambda_0 e(t) = 0. \tag{27}$$

Substituting $e(t) = R(t) - Y(t)$ yields

$$\ddot{R}(t) - \ddot{Y}(t) + \lambda_1 \left[\dot{R}(t) - \dot{Y}(t)\right] + \lambda_0 e(t) = 0. \tag{28}$$

From the process model in Equation (24), the second derivative of the output can be expressed as

$$\ddot{Y}(t) = \frac{K}{t_0\tau} U(t) - \frac{t_0 + \tau}{t_0\tau}\dot{Y}(t) - \frac{Y(t)}{t_0\tau}. \tag{29}$$

Substituting Equation (29) into Equation (28) and solving for $U(t)$ gives the general continuous control component:

$$U_C(t) = \left(\frac{t_0\tau}{K}\right)\left[\left(\frac{t_0 + \tau}{t_0\tau} - \lambda_1\right)\dot{Y}(t) + \frac{Y(t)}{t_0\tau} + \lambda_0 e(t) + \ddot{R}(t) + \lambda_1 \dot{R}(t)\right]. \tag{30}$$

For a constant reference, or to simplify the implementation, the reference derivatives are neglected:

$$\dot{R}(t) = 0, \qquad \ddot{R}(t) = 0. \tag{31}$$

Consequently, the continuous control component becomes

$$U_C(t) = \left(\frac{t_0\tau}{K}\right)\left[\left(\frac{t_0+\tau}{t_0\tau} - \lambda_1\right)\dot{Y}(t) + \frac{Y(t)}{t_0\tau} + \lambda_0 e(t)\right]. \tag{32}$$

According to the conventional FOPDT-based formulation, the parameter λ_1 is selected as [10]

$$\lambda_1 = \frac{t_0+\tau}{t_0\tau}. \tag{33}$$

Therefore,

$$\left(\frac{t_0+\tau}{t_0\tau} - \lambda_1\right) = 0. \tag{34}$$

Substituting Equation (34) into Equation (32) gives the reduced expression for the continuous component:

$$U_C(t) = \left(\frac{t_0\tau}{K}\right)\left[\frac{Y(t)}{t_0\tau} + \lambda_0 e(t)\right]. \tag{35}$$

Similarly, the conventional formulation suggests selecting λ_0 as [10]

$$\lambda_0 = \frac{1}{4}\left(\frac{t_0+\tau}{t_0\tau}\right)^2. \tag{36}$$

Equation (35) represents the continuous component of the SMC law. It compensates for the nominal process dynamics and is obtained by imposing $\dot{S}(t) = 0$. In the proposed hybrid controller, this component is retained, whereas the conventional discontinuous action is replaced by an interval Type-2 fuzzy logic system and then refined experimentally, since the original FOPDT tuning assumes two real poles whereas the identified plant is underdamped. The final sliding-surface parameters used in the experiments are reported in Table 4.

Discontinuous Component of the IT2FL-SMC Controller

Once the sliding surface $S(t)$ in Equation (25) and the continuous component $u_c(t)$ have been defined, the remaining part of the controller corresponds to the reaching action. In a conventional SMC, this action is generated by a switching function. In the proposed IT2FL-SMC controller, the switching function is replaced by the output of an interval Type-2 fuzzy logic system. This modification preserves the sliding-mode reaching criterion while avoiding the direct application of an ideal switching signal to the actuator.

The total control law is expressed as

$$u(t) = u_c(t) + u_d(t), \tag{37}$$

where $u_d(t)$ denotes the modified reaching component. For the proposed controller, this component is defined as

$$u_d(t) = \alpha u_{\mathrm{IT2}}(t), \qquad \alpha < 0. \tag{38}$$

Therefore, the complete control law becomes

$$u(t) = u_c(t) + \alpha u_{\mathrm{IT2}}(t). \tag{39}$$

In these expressions, $u_{\mathrm{IT2}}(t)$ is the signal generated by the interval Type-2 fuzzy logic system, whereas α is its output-scaling gain. The magnitude $|\alpha|$ determines the intensity of the reaching action, while its negative sign reverses the direction of the fuzzy-system output.

The negative gain is required because the tracking error is defined as $e(t) = R(t) - Y(t)$, as established in Equation (7). Consequently, a positive control action that increases $Y(t)$ enters the error dynamics, and therefore the sliding-surface dynamics, with a negative sign. Selecting $\alpha < 0$ preserves the required corrective direction without changing the orientation of the fuzzy consequents.

The fuzzy output $u_{\mathrm{IT2}}(t)$ is not designed as an independent control action. Instead, it provides a smooth approximation of the conventional SMC reaching component. The contribution of this component to the sliding-surface dynamics can be written as

$$\dot{S}(t)\big|_{u_d} = -u_d(t). \tag{40}$$

For this component to reduce the absolute value of the sliding surface, the following condition must be satisfied:

$$S(t)u_d(t) > 0. \tag{41}$$

Substituting $u_d(t) = \alpha u_{\mathrm{IT2}}(t)$ gives

$$\alpha S(t)u_{\mathrm{IT2}}(t) > 0. \tag{42}$$

Since $\alpha < 0$, dividing the inequality by α reverses its direction. Hence, the fuzzy-system output must satisfy

$$S(t)u_{\mathrm{IT2}}(t) < 0. \tag{43}$$

Although $u_{\mathrm{IT2}}(t)$ has a sign opposite to that of the sliding surface, the reaching component effectively applied to the plant satisfies

$$S(t)u_d(t) = \alpha S(t)u_{\mathrm{IT2}}(t) > 0, \tag{44}$$

because both α and $S(t)u_{\mathrm{IT2}}(t)$ are negative.

To verify the stability of the reaching action, the following Lyapunov candidate function is considered:

$$V(t) = \frac{1}{2}S^2(t). \tag{45}$$

Its time derivative is

$$\dot{V}(t) = S(t)\dot{S}(t). \tag{46}$$

The contribution of the fuzzy reaching component to the Lyapunov derivative is

$$\dot{V}(t)\big|_{u_d} = -S(t)u_d(t). \tag{47}$$

Substituting $u_d(t) = \alpha u_{\mathrm{IT2}}(t)$ yields

$$\dot{V}(t)\big|_{u_d} = -\alpha S(t)u_{\mathrm{IT2}}(t). \tag{48}$$

Because

$$\alpha < 0 \tag{49}$$

and

$$S(t)u_{\mathrm{IT2}}(t) < 0, \tag{50}$$

it follows that

$$\alpha S(t)u_{\mathrm{IT2}}(t) > 0, \tag{51}$$

and therefore

$$-\alpha S(t)u_{\mathrm{IT2}}(t) < 0. \tag{52}$$

Thus, the fuzzy reaching component contributes negatively to the derivative of the Lyapunov function. Provided that $|\alpha|$ is sufficiently large to dominate the effects of bounded uncertainties and disturbances, the following condition is satisfied:

$$\dot{V}(t) < 0, \tag{53}$$

or, equivalently,

$$S(t)\dot{S}(t) < 0, \qquad S(t) \neq 0. \tag{54}$$

The previous inequalities establish that the fuzzy reaching term makes $\dot{V}(t) < 0$, but they do not yet quantify how large the scaling gain α must be. To make this explicit, the mismatch between the nominal model used to derive $u_c(t)$ and the real plant is lumped into a bounded disturbance term. Writing the sliding-surface dynamics under the complete control law gives

$$\dot{S}(t) = \underbrace{\left(\dot{S}(t)\right)\big|_{u_c}}_{d(t)} + \left(\dot{S}(t)\right)\big|_{u_d}, \tag{55}$$

where $\left(\dot{S}\right)|_{u_c}$ collects the residual dynamics that the equivalent control does not cancel on the real plant—parametric uncertainty, unmodeled dynamics, and the external eccentric-load disturbance. This residual is assumed to be bounded,

$$\left|d(t)\right| \leq D, \qquad D > 0, \tag{56}$$

which is a standard and physically reasonable assumption, since the plant operates around an equilibrium point and the applied loads are finite. This formulation also clarifies the roles of the two terms: the equivalent component $u_c(t)$ compensates the nominal dynamics, whereas the fuzzy reaching component $u_d(t)$ is required to dominate only the residual $d(t)$ rather than the full plant dynamics.

Substituting the reaching contribution $\left(\dot{S}\right)|_{u_d} = -u_d(t) = -\alpha\, u_{\mathrm{IT2}}(t)$ into the Lyapunov derivative $\dot{V} = S\dot{S}$ yields

$$\dot{V}(t) = S(t)\, d(t) - \alpha\, S(t)\, u_{\mathrm{IT2}}(t). \tag{57}$$

By the reaching condition already established in Equation (43), the product $S(t)\, u_{\mathrm{IT2}}(t)$ is negative whenever $S(t) \neq 0$. Its magnitude admits a lower bound of the form $|S(t)\, u_{\mathrm{IT2}}(t)| \geq \mu\, |S(t)|$, with $\mu > 0$ determined by the normalized fuzzy output.

Using $|d(t)| \leq D$:

$$\dot{V}(t) \leq |S(t)|\, D - |\alpha|\, \mu\, |S(t)| = -\left(|\alpha|\, \mu - D\right) |S(t)|. \tag{58}$$

Hence, the η-reachability condition $\dot{V}(t) \leq -\eta\, |S(t)|$, with $\eta > 0$, is guaranteed provided that

$$|\alpha| \geq \frac{D + \eta}{\mu}. \tag{59}$$

Condition (59) gives an explicit lower bound on the fuzzy scaling gain: $|\alpha|$ must exceed the disturbance bound D (scaled by $1/\mu$) by a margin that fixes the finite-time reaching rate η. This makes precise the earlier requirement that $|\alpha|$ be "sufficiently large," and shows that the closed loop remains stable for any disturbance whose magnitude satisfies $D < |\alpha|\, \mu - \eta$. In practice, $|\alpha|$ was selected experimentally above this bound, which is consistent with the robust disturbance rejection observed in Section 3.

Under this condition, the magnitude of the sliding surface decreases and the system trajectory is driven toward $S(t) = 0$.

The fuzzy system has two inputs: the sliding surface $S(t)$ and its derivative $\dot{S}(t)$. Its output is the fuzzy consequent $u_{\mathrm{IT2}}(t)$, which determines the reaching action after being scaled by α. Therefore, the fuzzy system has a MISO structure.

The consequent signs are assigned according to the reaching condition in Equation (54) and the sign relationship in Equation (43). Specifically,

$$S(t) > 0 \Rightarrow u_{\mathrm{IT2}}(t) < 0 \Rightarrow u_d(t) = \alpha u_{\mathrm{IT2}}(t) > 0, \tag{60}$$

whereas

$$S(t) < 0 \Rightarrow u_{\mathrm{IT2}}(t) > 0 \Rightarrow u_d(t) = \alpha u_{\mathrm{IT2}}(t) < 0. \tag{61}$$

The derivative $\dot{S}(t)$ is included as the second fuzzy-system input to determine whether the system trajectory is approaching or moving away from the sliding surface. While $S(t)$ indicates the current position of the trajectory relative to $S(t) = 0$, $\dot{S}(t)$ describes its direction of motion.

When $S(t)$ and $\dot{S}(t)$ have the same sign,

$$S(t)\dot{S}(t) > 0, \tag{62}$$

the magnitude of the sliding surface is increasing and the trajectory is moving away from $S(t) = 0$. Consequently, the fuzzy system must produce an output of greater magnitude and with a sign opposite to that of $S(t)$. The negative gain α then reverses this signal and generates the required corrective reaching action.

Conversely, when $S(t)$ and $\dot{S}(t)$ have opposite signs,

$$S(t)\dot{S}(t) < 0, \tag{63}$$

the trajectory is approaching the sliding surface. In this region, the magnitude of the fuzzy output can be reduced to prevent excessively rapid crossings and mitigate oscillations around $S(t) = 0$.

The membership functions used for the inputs of the IT2FL-SMC reaching component are the same as those previously defined for the interval Type-2 fuzzy logic controller. Likewise, the output is represented by interval singleton consequents. Maintaining the same distribution of input and output membership functions enables the performance of the different control structures to be compared under equivalent fuzzy-system configurations.

The Lyapunov-based sign conditions lead to a consequent assignment consistent with the rule-base pattern used in the IT2FL controller. The main difference lies in the input variables, which are now $S(t)$ and $\dot{S}(t)$ rather than the tracking error and its derivative. Nevertheless, the rule-activation, inference, Type-reduction, and defuzzification procedures remain unchanged.

Accordingly, the discontinuous component of the IT2FL-SMC controller is derived from the previously developed interval Type-2 fuzzy logic controller by modifying its input variables and incorporating its scaled output as the reaching action within the SMC structure.

3. Experimental Results and Discussion

In this section, the experimental performance of the PID, Type-1 fuzzy, SMC, Type-1 fuzzy-SMC, IT2FL, and IT2FL-SMC controllers is compared. All tests were conducted at a sampling frequency of 100 Hz, corresponding to a sampling period of $T_s = 0.01$ s. The evaluation considered three scenarios: step-reference tracking and constant-reference track-

ing under the application and removal of downward and upward external disturbances. These tests assess the transient response, robustness, and disturbance-rejection capability of each controller.

The performance indices used for the comparison are defined below. The integral of the squared error (ISE) is computed as the sum of the squared error over the experimental interval. Because errors are penalized quadratically, large deviations have a greater influence on this index, particularly during transient operation. Therefore, lower ISE values indicate a better attenuation of large tracking errors [27]:

$$\text{ISE} = \sum_{k=0}^{N} e^2(k). \tag{64}$$

The integral of the absolute error (IAE) is the accumulated absolute tracking error over the test interval, irrespective of its sign. A lower IAE indicates that the system output remains closer to the desired reference throughout the experiment [27]:

$$\text{IAE} = \sum_{k=0}^{N} |e(k)|. \tag{65}$$

The total variation of the control input (TVU) quantifies the accumulated changes in the control action. It provides a measure of the control effort required under reference changes and external disturbances. Lower TVU values are associated with smoother actuation and fewer abrupt changes applied to the actuator [28]:

$$\text{TVU} = \sum_{k=1}^{N} |u(k) - u(k-1)|. \tag{66}$$

All three indices are computed as discrete sums over the same 60 s window, sampled at $T_s = 0.01$ s, so they are reported in the units of the summed quantity: degrees for IAE, squared degrees for ISE, and amperes for TVU. Since every controller is evaluated over the same window and sampling period, the indices are directly comparable across controllers without further normalization. The settling time is measured using a $\pm 5\%$ band around the final reference value.

The controllers were tuned sequentially, following a procedure similar to PID calibration: the proportional contribution was adjusted first, followed by the derivative and integral contributions, while the system response was evaluated at each stage. To ensure a fair comparison, controllers with equivalent architectures were assigned the same gains. In particular, the Type-1 fuzzy and IT2FL controllers share a MISO PD+I fuzzy structure; therefore, the gains tuned for the Type-1 controller were also used for the IT2FL controller to isolate the effect of interval Type-2 fuzzy logic. The tuning parameters are listed in Tables 4–6.

Table 4. Tuning parameters of the sliding-mode-based controllers.

Controller	Val_1	Val_2	K	K_{Dvar}
SMC	0.25	0.45	0.6	4.2
Type-1 Fuzzy-SMC	0.25	0.45	0.6	–
IT2FL-SMC	0.25	0.45	0.6	–

Table 4 summarizes the parameters used for the experimental tuning of the SMC-based controllers. The values initially obtained from the second-order plant model were used as a theoretical reference for the controller design.

The parameters Val_1 and Val_2 provide an equivalent parametrization of the sliding-surface coefficients λ_1 and λ_0. Their theoretical reference values follow from the second-order plant model through:

$$\left(\frac{\mathrm{Val}_1}{\mathrm{Val}_2}\right)_{\mathrm{theo}} = \frac{t_0 + \tau}{t_0 \tau}, \tag{67}$$

which was used as the starting point for the design. As stated above, the final values reported in Table 4 were retuned experimentally to account for the nonlinearities and unmodeled dynamics of the real plant, and therefore do not satisfy the nominal relation exactly.

For the conventional SMC, an additional tuning factor, denoted as K_{Dvar}, was introduced in the robust control term. Thus, the implemented control law can be expressed as [10]

$$U(t) = \left(\frac{t_0 \tau}{K}\right)\left[\frac{Y(t)}{t_0 \tau} + \lambda_0 e(t)\right] + (K_D K_{Dvar})\frac{S(t)}{|S(t)| + \delta}. \tag{68}$$

The factor K_{Dvar} acts as a multiplicative adjustment of the nominal switching gain K_D and was included to allow its magnitude to be modified during experimental tuning. Increasing K_{Dvar} strengthens the corrective action of the SMC and improves its ability to reject disturbances, whereas reducing it produces a smoother control action with lower control effort. Therefore, its final value was selected experimentally as a compromise between tracking performance, robustness, and control effort. This auxiliary factor was only required in the conventional SMC. In the Type-1 Fuzzy-SMC and IT2FL-SMC controllers, the switching action of the conventional SMC is replaced by the Type-1 and interval Type-2 fuzzy inference systems, respectively. Consequently, the explicit adjustment provided by K_{Dvar} is no longer required in these controllers.

Table 5 presents the gains used by the Type-1 fuzzy and IT2FL controllers under the common PD+I architecture, together with the tuning constants of the discontinuous fuzzy action in the fuzzy-SMC controllers.

Table 5. Tuning parameters of the fuzzy controllers.

Controller	$\mathbf{K_e}$	$\mathbf{K_d}$	$\boldsymbol{\alpha}$	$\boldsymbol{\beta}$
Type-1 Fuzzy	4	4	0.5	3
IT2FL	4	4	0.5	3
Type-1 Fuzzy-SMC	4	0.001	−1.2	–
IT2FL-SMC	4	0.001	−1.2	–

Table 6. Tuning parameters of the PID controller.

Controller	$\mathbf{K_p}$	$\mathbf{K_i}$	$\mathbf{K_d}$
PID	1.56	3.98	1.17

The Type-1 fuzzy-SMC and IT2FL-SMC controllers were also implemented with the same control structure and tuning parameters. Consequently, the differences in their responses can be attributed mainly to the incorporation of the footprint of uncertainty rather than to architectural or tuning changes.

3.1. Footprint-of-Uncertainty Tuning for the IT2FL and IT2FL-SMC Controllers

The footprint of uncertainty was calibrated experimentally while preserving the PD+I gains, the interval Type-2 fuzzy structure, and the reference trajectory. Thus, changes in the system response were associated only with the selected FOU.

The IT2FL controller was tested with FOU values of 0.05, 0.15, 0.25, and 0.50. For each configuration, the lower membership functions were modified while the upper membership functions, linguistic variables, distribution, and universe of discourse remained unchanged. Figure 6 shows the resulting responses.

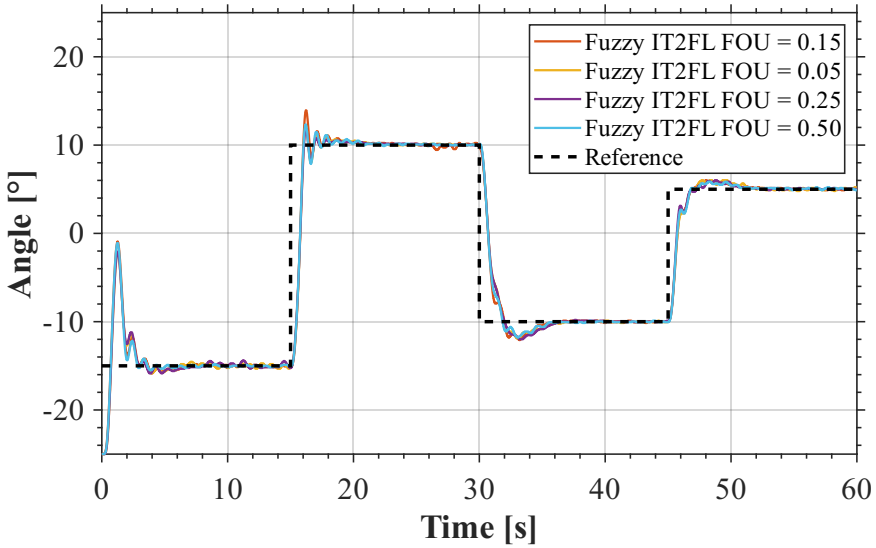


Figure 6. Comparison of the IT2FL responses for different footprint-of-uncertainty values.

To make the FOU choice systematic rather than qualitative, the three indices were combined into a single normalized cost

$$J(\Delta_{\mathrm{FOU}}) = \frac{1}{3}\left(\frac{\mathrm{IAE}}{\mathrm{IAE}_{\max}} + \frac{\mathrm{ISE}}{\mathrm{ISE}_{\max}} + \frac{\mathrm{TVU}}{\mathrm{TVU}_{\max}}\right), \tag{69}$$

where each index is divided by its largest value across the tested configurations. IAE and ISE measure tracking accuracy and TVU measures control smoothness, and the three are weighted equally. A narrow footprint brings the response close to a type-1 controller, while a wide one over-smooths the inference and makes the response sluggish and more oscillatory. The value $\Delta_{\mathrm{FOU}} = 0.25$ gives the smallest J (Table 7), so it was selected.

Table 7. Performance indices for different FOU values in the IT2FL controller.

FOU Configuration	IAE	ISE	TVU	J
IT2FL with FOU = 0.15	76.27	855.51	702.14	0.996
IT2FL with FOU = 0.05	76.79	846.80	601.82	0.948
IT2FL with FOU = 0.25	76.20	842.78	571.56	0.929
IT2FL with FOU = 0.50	76.37	858.75	594.68	0.947

3.2. Reference-Change Tests

The first experiment evaluates the transient response of the controllers under step-reference changes, considering overshoot, response speed, settling time, and post-transient stability. The system starts from rest at $-25°$, and the reference changes to $-15°$ at $t = 0$ s. It then increases to $10°$ at $t = 15$ s, decreases to $-10°$ at $t = 30$ s, and finally increases to $5°$ at $t = 45$ s. This sequence evaluates the ability of each controller to respond to both upward and downward reference variations.

Figure 7 shows that all controllers track the desired trajectory, although their transient responses differ in overshoot, settling time, and oscillatory behavior. During the initial step, the IT2FL and Type-1 fuzzy-SMC controllers provide comparatively smooth transitions, with some oscillation near the reference.

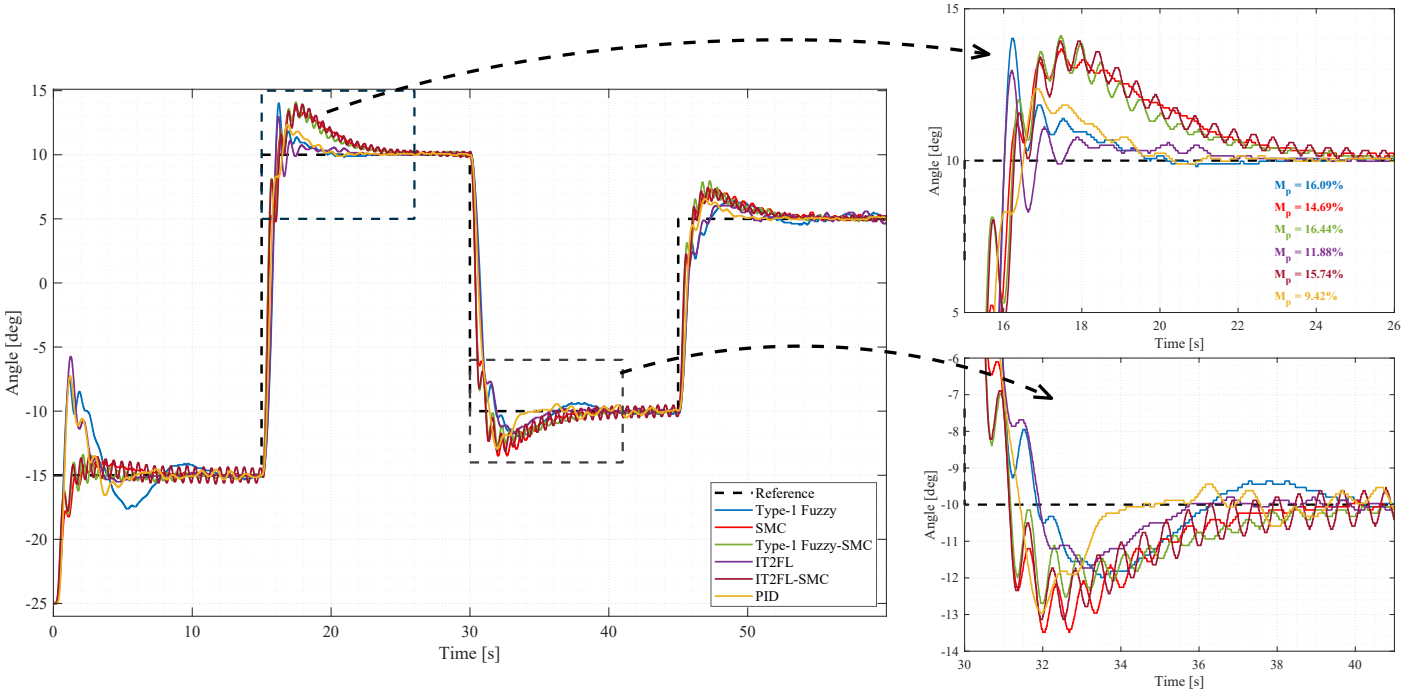


Figure 7. Dynamic responses of the controllers under reference variations.

For the upward change at $t = 15$ s, the PID controller produces the lowest overshoot, approximately 9.42%. The IT2FL controller follows with 11.88%, while maintaining a smooth transition. This result indicates that the interval Type-2 fuzzy structure can accommodate system uncertainty without generating an excessively abrupt response. By contrast, the Type-1 fuzzy controller exhibits a more aggressive and oscillatory response, with an overshoot of approximately 16.09%. The SMC, Type-1 fuzzy-SMC, and IT2FL-SMC controllers produce overshoots of 14.69%, 16.44%, and 15.74%, respectively.

During the downward step at $t = 30$ s, the SMC-based controllers generate a sharper transient and greater oscillation before converging to the reference. The IT2FL controller instead provides a smoother and more gradual transition while retaining a competitive settling time. This behavior is advantageous when abrupt actuator commands are undesirable.

The control signals in Figure 8 support the previous observations. The IT2FL controller produces the most regular input, with less ripple and lower aggressiveness during reference changes. The PID signal is also relatively smooth, whereas the SMC-based controllers, particularly the Type-1 fuzzy-SMC and IT2FL-SMC, generate more active control actions. This increased activity can improve error correction and robustness, but it also raises the demand on the actuator.

Table 8 shows that the Type-1 fuzzy-SMC controller achieves the lowest IAE and ISE, with values of 68.83 and 525.81, respectively. However, its high TVU of 1353.50, overshoot of 16.44%, and settling time of 7.59 s indicate that the improvement in integral-error indices is obtained at the expense of a more oscillatory control input and a less favorable transient response.

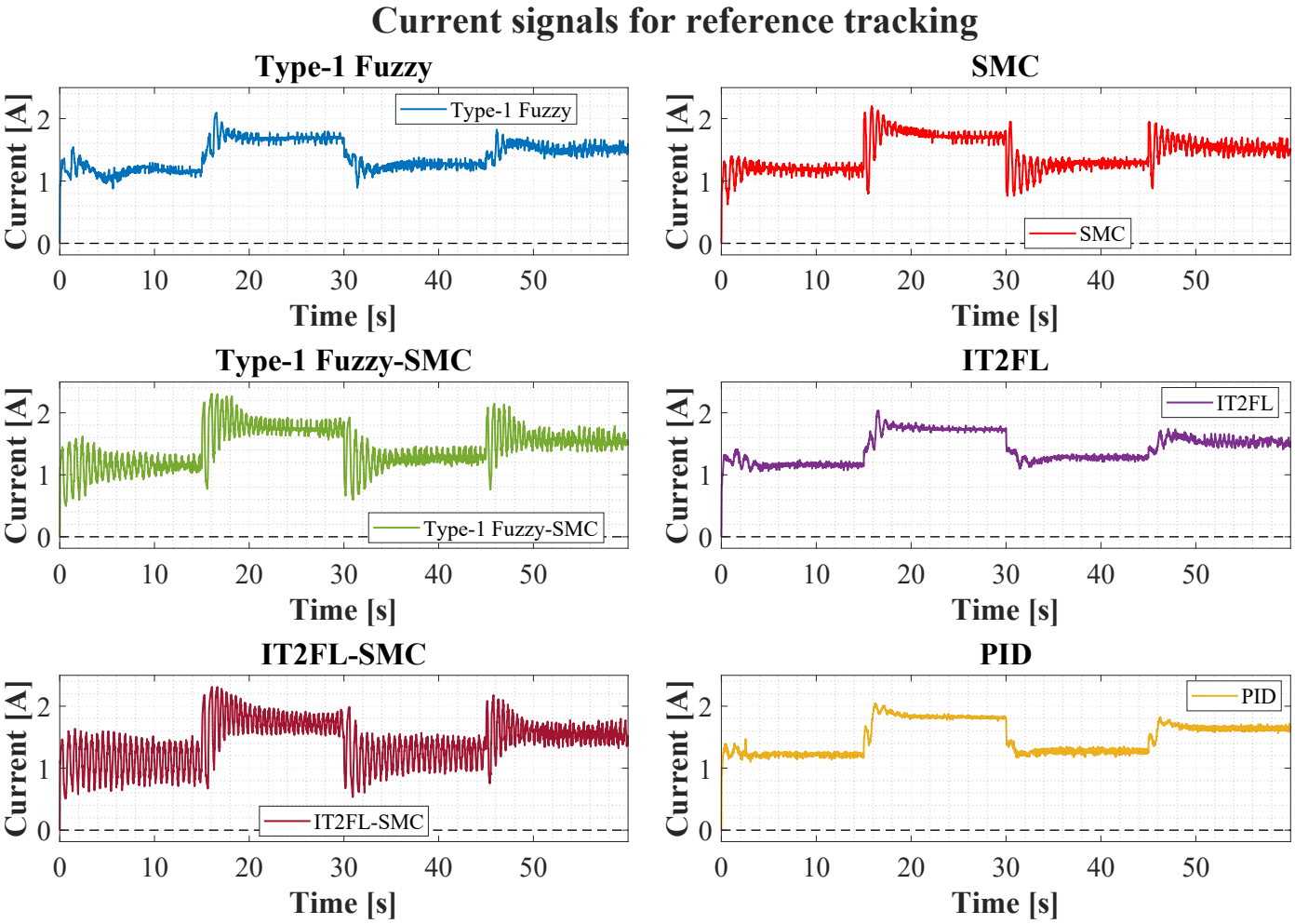


Figure 8. Control inputs generated under reference variations.

Table 8. Performance indices for the reference-tracking test.

Controller	IAE	ISE	TVU	M_p [%]	T_s [s]
PID	69.21	695.62	797.81	9.42	4.36
Type-1 Fuzzy	88.73	843.44	809.69	16.09	3.95
SMC	74.13	547.51	948.13	14.69	7.79
Type-1 Fuzzy-SMC	68.83	525.81	1353.50	16.44	7.59
IT2FL	73.21	790.21	543.30	11.88	3.83
IT2FL-SMC	74.23	554.87	1668.50	15.74	8.89

Note: The IAE, ISE, and TVU indices were calculated over a 60 s evaluation interval. The maximum overshoot and settling time correspond to the reference change evaluated between 15 s and 30 s.

To give a sense of how consistent each controller is, rather than relying on a single transient, the tracking test is treated as a set of repeated transitions. It applies three reference steps ($+10°$, $-10°$, and $+5°$). The initial motion from rest to the first setpoint is not included, because the arm starts from a standstill with the motor off: that first transient is dominated by the start-up dynamics and the small $10°$ span, so its overshoot is much larger and not comparable to a normal reference change. Table 9 reports the mean and standard deviation of the overshoot and settling time over the three comparable steps. The IT2FL keeps the lowest average overshoot and the shortest average settling time, while the IT2FL-SMC shows the most consistent overshoot, both consistent with the individual tests.

Table 9. Consistency of the transient response across the three reference steps of the tracking test (mean ± standard deviation over the $+10^\circ$, -10°, and $+5^\circ$ steps).

Controller	M_p [%]	T_s [s]
PID	11.31 ± 2.78	3.12 ± 1.18
Type-1 Fuzzy	12.03 ± 3.52	3.25 ± 1.09
SMC	15.30 ± 1.04	5.56 ± 2.01
Type-1 Fuzzy-SMC	16.65 ± 3.25	5.06 ± 2.19
IT2FL	9.19 ± 2.60	2.51 ± 1.15
IT2FL-SMC	15.15 ± 0.54	5.53 ± 2.91

The IT2FL controller provides the most balanced nominal tracking performance. It achieves the lowest TVU, 543.30, and the shortest settling time, 3.83 s, together with a moderate overshoot of 11.88%, the second-lowest value after the PID controller. Compared with the Type-1 fuzzy controller, the IT2FL reduces IAE, ISE, TVU, overshoot, and settling time. These results show that the footprint of uncertainty improves response speed and smoothness while reducing actuator demand.

The IT2FL-SMC controller yields IAE and ISE values close to those of the SMC and Type-1 fuzzy-SMC controllers; nevertheless, it has the largest TVU, 1668.50, and the longest settling time, 8.89 s. Thus, under nominal reference tracking, the interval Type-2 extension of the SMC structure does not significantly improve the transient response and requires greater control effort. Its tuning, however, was selected not only for nominal tracking but also to preserve stability and disturbance-rejection capability under severe external loads. Reducing its fuzzy gain decreased oscillations but also weakened robustness; therefore, the selected parameters represent a compromise between tracking performance and disturbance rejection.

3.3. Downward-Disturbance Rejection Test

A mass of 0.018 kg was used to generate the downward external disturbance. The distance from the rotation axis to the center of mass was 0.085 m, with the mass placed near the propeller. Using $\tau_p = m_p g d_p$, the resulting torque was 0.0150 N m.

The mass was added at $t = 20$ s and removed at $t = 40$ s while the reference was fixed at 0°. Adding the load causes an abrupt downward deviation, whereas removing it produces an upward transient. Because the disturbance was introduced by a real external mass of 18 g rather than through software, this experiment directly evaluates the robustness of each controller under a physical load variation.

Figure 9 shows the negative deviation produced at approximately $t = 20$ s. The Type-1 fuzzy and IT2FL controllers initially react more gradually than the SMC-based strategies, resulting in a less immediate rejection of the disturbance. Nevertheless, both eventually compensate for the error within a comparable interval.

The SMC-based controllers respond more actively to the load-induced deviation. The conventional SMC produces a direct correction, while the Type-1 fuzzy-SMC controller rapidly reduces the error after the initial negative transient. The IT2FL-SMC provides the best overall rejection, recovering the reference more rapidly and limiting the deviation caused by the external load. This behavior reflects the combined robustness of sliding-mode control and the uncertainty-handling capability of interval Type-2 fuzzy logic.

When the mass is removed at approximately $t = 40$ s, all controllers experience a positive deviation. The IT2FL-SMC again returns rapidly to the reference without producing an excessive overshoot. The Type-1 fuzzy and IT2FL responses are smoother, although the IT2FL exhibits a temporary positive peak before converging. Overall, the SMC-based

strategies provide stronger rejection, whereas the IT2FL offers a smoother response with lower actuator demand.

Figure 10 shows the control signals during the application and removal of the load. The PID and IT2FL controllers generate smoother inputs, which reduce actuator demand but are associated with a slightly slower initial reaction. The Type-1 fuzzy controller follows a similar pattern, although its control signal is more aggressive and its disturbance response is less favorable than that of the IT2FL.

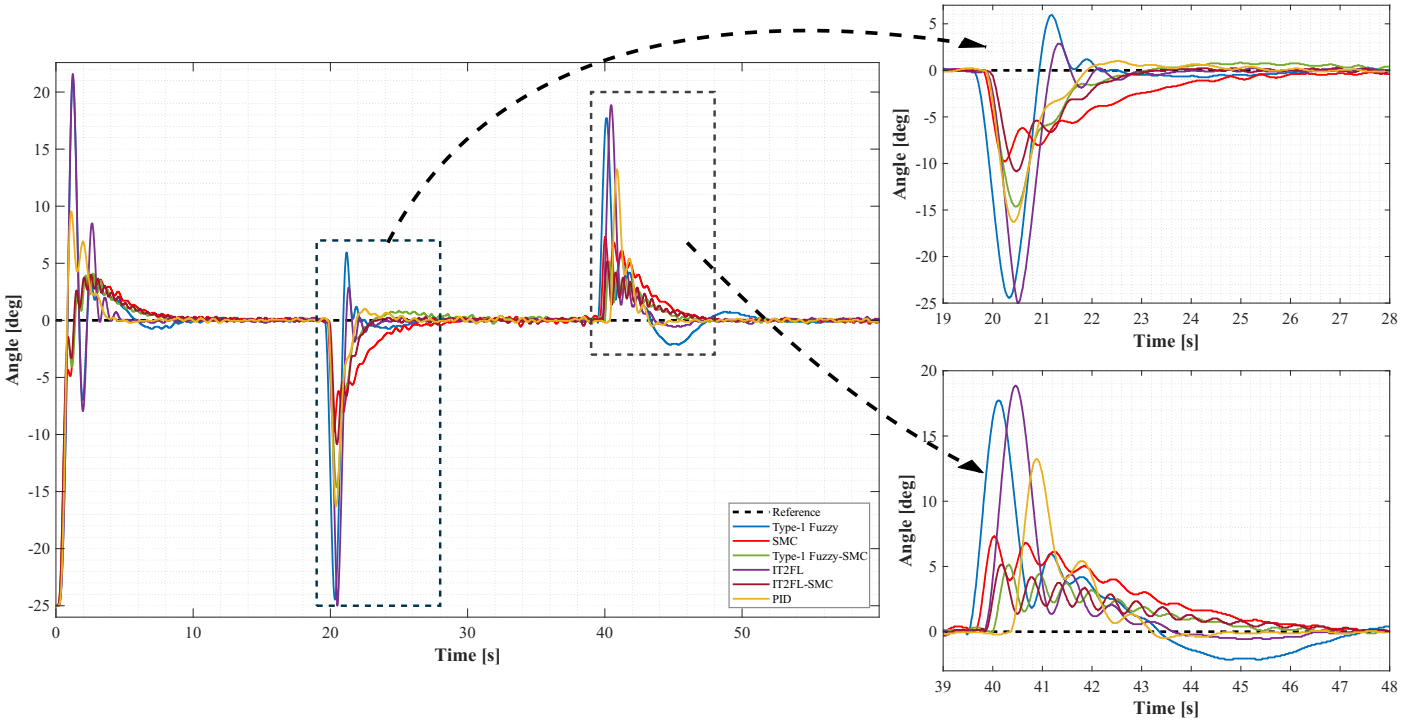


Figure 9. Dynamic responses of the controllers under a fixed reference and a downward disturbance.

The IT2FL-SMC produces the most active signal during both compensation intervals. This behavior enables a faster recovery and limits excessive upward or downward motion of the arm. Despite the increased activity, the current stays below the actuator's saturation limit of approximately 3 A, so no saturation occurs and the controller maintains acceptable actuation while providing strong disturbance rejection.

As shown in Table 10, the IT2FL-SMC achieves the lowest IAE and ISE, with values of 54.32 and 430.40, respectively. This confirms its superior ability to reduce both accumulated error and large transient deviations. The Type-1 fuzzy-SMC ranks second in these indices, supporting the advantage of combining fuzzy logic with sliding-mode control for disturbance rejection.

Table 10. Controller performance indices for downward-load disturbance rejection.

Controller	IAE	ISE	TVU	M_p [%]	T_s [s]
PID	59.31	646.15	623.36	16.35	4.36
Type-1 Fuzzy	89.53	1094.00	1029.90	24.43	5.07
SMC	75.04	534.83	1069.70	9.76	5.93
Type-1 Fuzzy-SMC	57.70	493.11	1245.70	14.68	2.84
IT2FL	75.81	1069.50	776.51	24.87	2.72
IT2FL-SMC	54.32	430.40	1458.50	10.81	2.69

Note: The IAE, ISE, and TVU indices were calculated over a 60 s evaluation interval. The maximum overshoot M_p and settling time T_s were determined within the 20–35 s window corresponding to the downward-load disturbance.

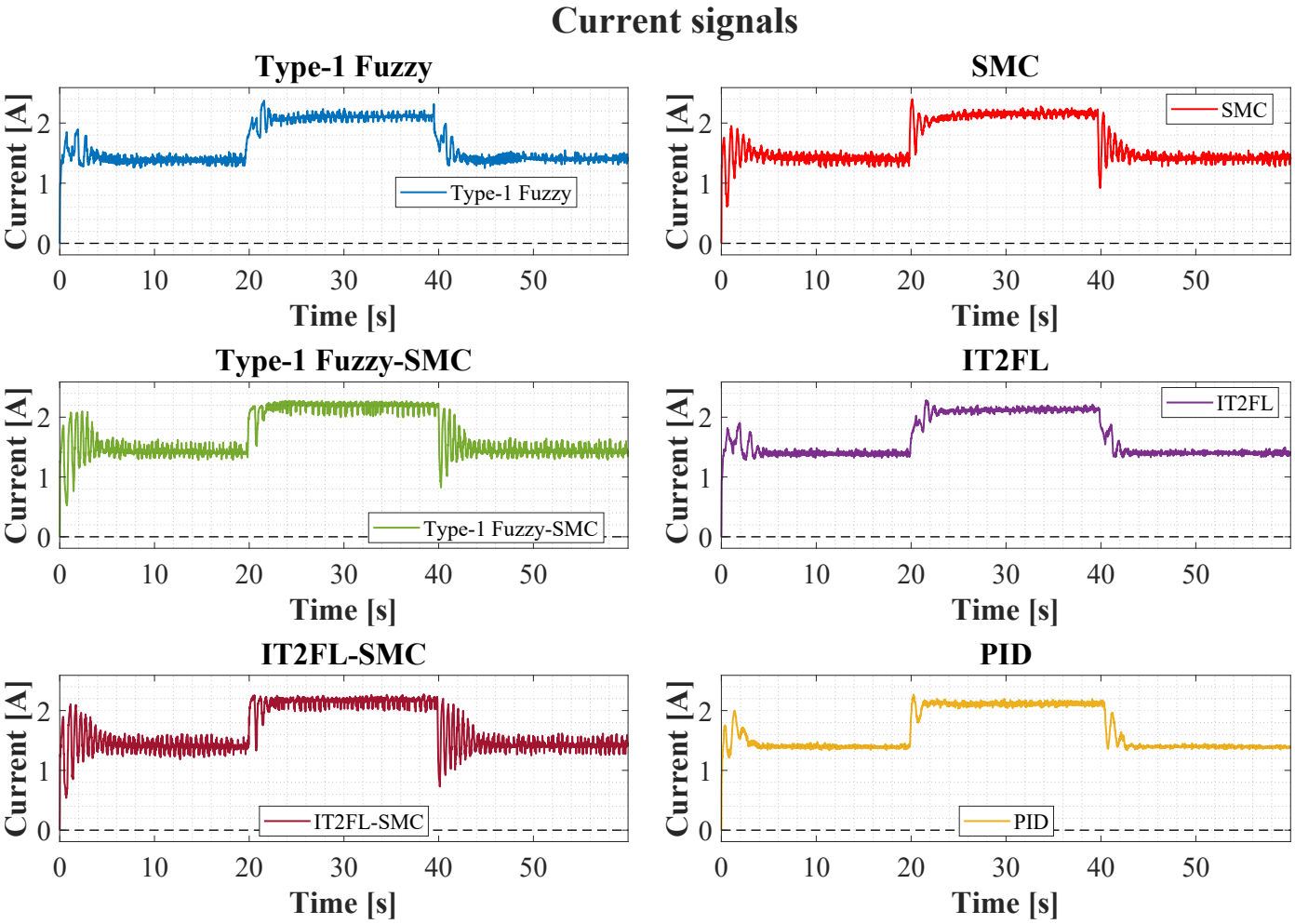


Figure 10. Control inputs generated under a fixed reference and a downward eccentric disturbance.

Compared with the Type-1 fuzzy controller, the IT2FL reduces IAE and TVU and shortens the settling time from 5.07 s to 2.72 s. However, it produces the largest overshoot, 24.87%, indicating a substantial initial deviation before stabilization. Thus, the IT2FL offers fast recovery and relatively smooth actuation, although its initial response to this disturbance is less well damped.

The IT2FL-SMC also outperforms the PID controller in IAE and, more clearly, in ISE. It reduces the settling time from 4.36 s to 2.69 s and the overshoot from 16.35% to 10.81%. Although the conventional SMC obtains a slightly lower overshoot of 9.76%, it requires 5.93 s to settle. Therefore, the IT2FL-SMC provides the best compromise among rapid recovery, error reduction, and limitation of the maximum deviation, at the cost of a higher TVU caused by its more active control action.

3.4. Upward-Disturbance Rejection Test

The upward disturbance was generated using the same 0.018 kg mass. In this test, the center of mass was located 0.060 m from the rotation axis, directly above the counterweight. From $\tau_p = m_p g d_p$, the applied torque was 0.0106 N m.

The mass was added at $t = 20$ s and removed at $t = 40$ s while the reference remained fixed at 0°. Adding the load produces a sudden upward motion of the arm, whereas removing it causes a downward deviation. Together with the previous experiment, this test evaluates controller robustness under physical disturbances acting in opposite directions.

Figure 11 shows the positive deviation generated at $t = 20$ s. The Type-1 fuzzy, IT2FL, and PID controllers exhibit larger positive peaks than the SMC-based strategies. Even so, the IT2FL recovers rapidly, with a response comparable to that of the Type-1 fuzzy-SMC but with a smoother control action.

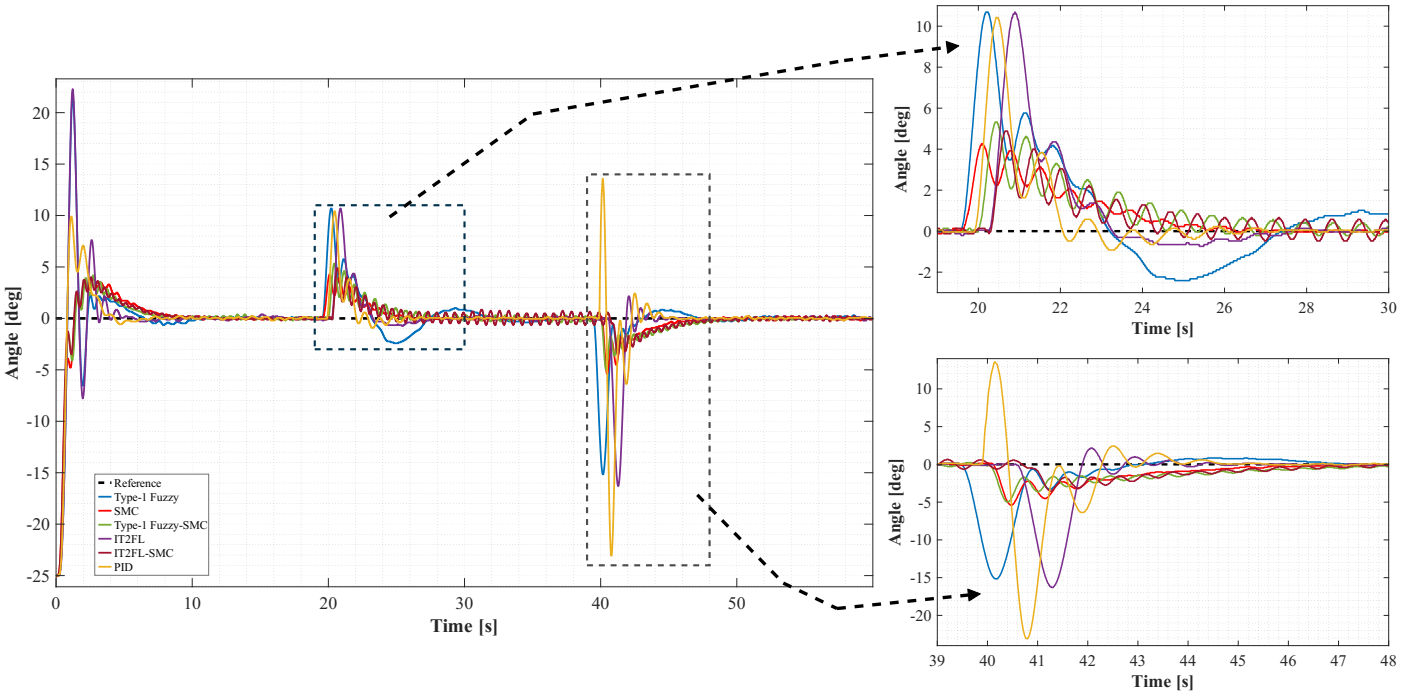


Figure 11. Dynamic responses of the controllers under a fixed reference and an upward eccentric disturbance.

The conventional SMC and Type-1 fuzzy-SMC limit the initial deviation more effectively, although they require more active control inputs. The IT2FL-SMC again provides the best overall disturbance rejection by reducing both the peak deviation and the interval during which the output remains away from the reference.

When the disturbance is removed at approximately $t = 40$ s, a negative deviation appears. The Type-1 fuzzy, IT2FL, and PID controllers produce more pronounced negative transients, whereas the SMC-based controllers limit this deviation through a more active correction. The IT2FL-SMC maintains the best overall response, combining a limited deviation with a stable return to the reference.

Figure 12 shows that applying the upward load requires a reduction in the control input to compensate for the deviation. The IT2FL again generates a comparatively smooth signal, avoids saturation, and suppresses large oscillations while recovering within a competitive interval.

The IT2FL-SMC signal contains faster variations and greater ripple during the application and removal of the disturbance. This increased activity explains the smaller peak deviations observed in the output response. The PID signal is relatively smooth, but its tracking response is more oscillatory, particularly near $t = 40$ s, where an abrupt increase occurs after the load is removed. Overall, the IT2FL-SMC is the most robust controller in this experiment, whereas the IT2FL offers the smoother and less demanding control action.

Table 11 shows that the IT2FL-SMC achieves the lowest IAE and ISE under the upward disturbance, with values of 51.05 and 353.60, respectively. Its TVU, however, is approximately twice that of the PID controller. This increase results from the more active control signal required by the combined sliding-mode and interval Type-2 fuzzy structure

to suppress the load-induced deviation. The higher TVU therefore represents the trade-off between actuator demand and improved disturbance rejection.

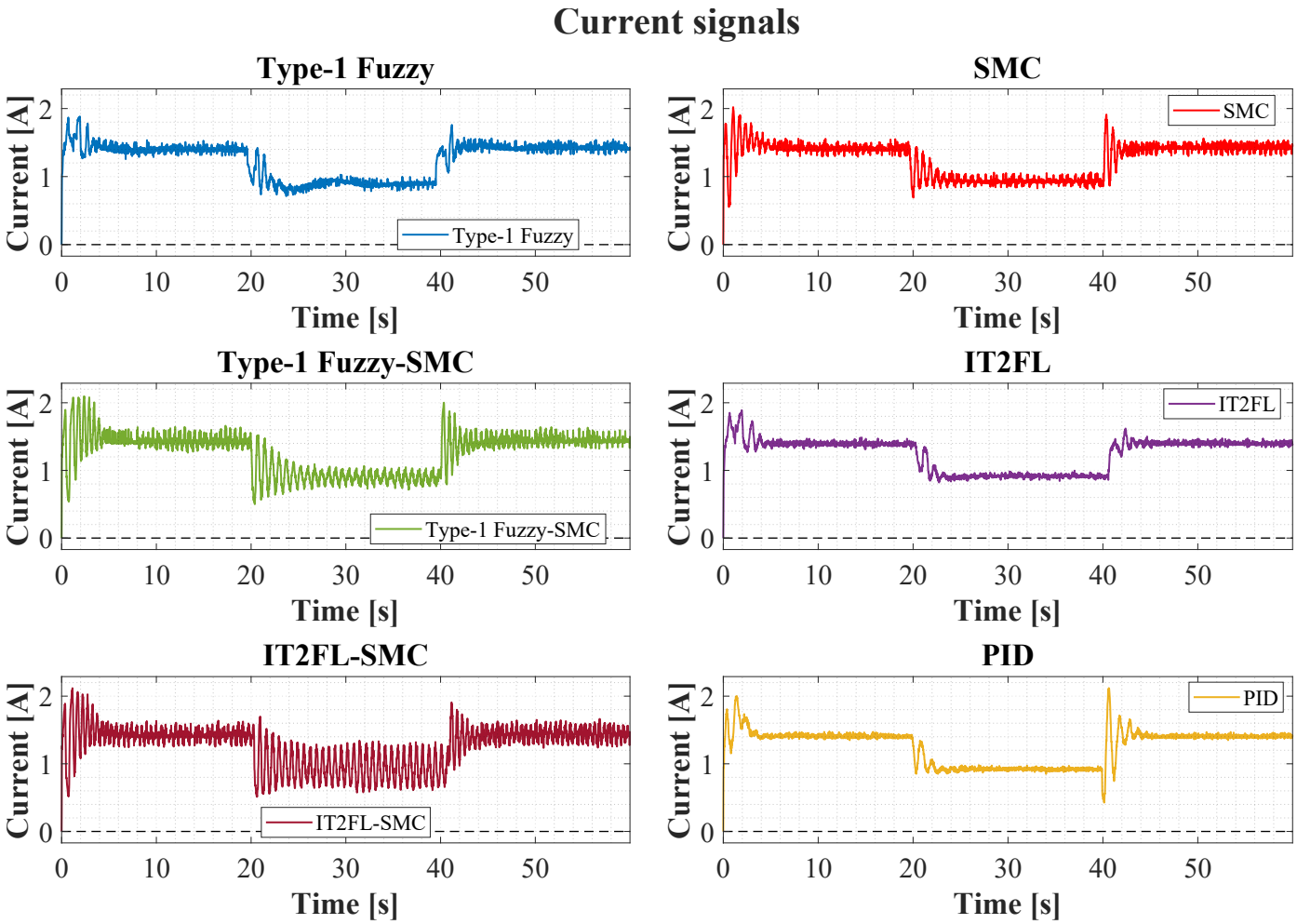


Figure 12. Control inputs generated under a fixed reference and an upward eccentric disturbance.

Table 11. Controller performance indices for upward-load disturbance rejection.

Controller	IAE	ISE	TVU	M_p [%]	T_s [s]
PID	62.88	740.68	669.88	10.46	4.36
Type-1 Fuzzy	79.25	790.31	958.21	10.64	7.07
SMC	51.22	380.73	1039.10	4.22	4.54
Type-1 Fuzzy-SMC	53.01	391.78	1349.70	5.27	7.20
IT2FL	65.41	805.41	742.30	10.72	3.15
IT2FL-SMC	51.05	353.60	1632.20	4.92	5.28

Note: The IAE, ISE, and TVU indices were calculated over a 60 s evaluation interval. The maximum overshoot M_p and settling time T_s were determined within the 20–35 s window corresponding to the upward-load disturbance.

The conventional SMC produces the lowest overshoot, 4.22%, followed by the IT2FL-SMC with 4.92%. Hence, the sliding-mode-based strategies limit the maximum disturbance-induced deviation more effectively than the PID, Type-1 fuzzy, and IT2FL controllers, whose overshoots exceed 10%.

Although the IT2FL does not minimize IAE or ISE, it requires less control effort and achieves the shortest settling time, $T_s = 3.15$ s. The IT2FL-SMC settles in 5.28 s, but combines the lowest accumulated errors with the second-lowest overshoot. Accordingly, the IT2FL-SMC is preferable when robust disturbance rejection and error reduction are the

primary objectives, whereas the IT2FL is more suitable when smoother actuation and faster settling are prioritized.

3.5. Qualitative Analysis of the Controllers

Table 12 summarizes the overall qualitative behavior of the evaluated controllers.

Table 12. Overall qualitative analysis of the controllers.

Controller	Stability	Overshoot/ Deviation	Control Input	Remarks
PID	High	Low to medium	Smooth	Produces a low TVU and a regular control action, but its disturbance-rejection capability is lower than that of the robust controllers.
Type-1 Fuzzy	Medium–high	Medium to high	Moderate	Maintains stability but exhibits larger accumulated errors and more pronounced transient deviations, particularly under disturbances.
SMC	High	Medium	High activity	Improves disturbance rejection compared with the PID and Type-1 fuzzy controllers, although it increases control-input variation.
Type-1 Fuzzy-SMC	High	Medium	High activity	Reduces the error in several tests, but requires a more active and demanding control signal.
IT2FL	High	Medium to high	Very smooth	Produces the lowest TVU during reference tracking and comparatively low TVU values under disturbances. It is suitable when smooth actuation and reduced actuator demand are prioritized.
IT2FL-SMC	High	Medium	High activity	Achieves the lowest IAE and ISE under both downward and upward disturbances. It provides the strongest rejection of eccentric loads, although at the expense of greater control-input variation.

The IT2FL and IT2FL-SMC controllers provide complementary advantages. The IT2FL is distinguished by its smooth control signal and low total variation, particularly in the reference-tracking test, where it obtains the lowest TVU. This result indicates that interval Type-2 fuzzy logic improves uncertainty handling without imposing abrupt current variations on the actuator.

The principal advantage of the IT2FL-SMC appears under external disturbances. It achieves the lowest IAE and ISE for both downward and upward loads, outperforming the conventional SMC and Type-1 fuzzy-SMC in the main error indices. These results confirm that integrating interval Type-2 fuzzy logic with sliding-mode control strengthens robustness against eccentric loads that disturb the arm equilibrium.

The higher TVU of the IT2FL-SMC is caused by the more active control action required to compensate rapidly for disturbance-induced angular deviations. Consequently, the IT2FL is more appropriate when smooth actuation and reduced actuator demand are prioritized, whereas the IT2FL-SMC is the preferred alternative when robust external-disturbance rejection is the main objective.

One aspect that cannot be overlooked relates to measurement noise. The angle is obtained from an encoder, and calculating its derivative amplifies the signal's quantization noise. The TVU metric reflects this phenomenon; specifically, if a controller allows a greater amount of that noise to reach the actuator, its TVU value increases. This is one reason why SMC-based controllers—and the IT2FL-SMC in particular—outperform the IT2FL. The Footprint of Uncertainty (FOU) works to the controller's advantage by smoothing the

inference process, allowing the IT2FL signal to remain clean even in the presence of a noisy derivative. A proper test involving noise injection would confirm this point and remains a task for future work.

4. Conclusions

The proposed IT2FL controller improved the performance of the Type-1 fuzzy controller under the same PD+I structure and tuning conditions. The footprint of uncertainty enhanced the controller's ability to accommodate variations in the system dynamics, resulting in smoother control action, lower TVU, and improved reference-tracking performance. These results confirm that the observed improvements are mainly associated with the interval Type-2 fuzzy formulation rather than with changes in the controller architecture.

The IT2FL-SMC controller achieved the best disturbance rejection, with the lowest IAE and ISE under both load directions, at the expense of the highest total variation of the control input among the evaluated controllers; the control signal stayed below the actuator's saturation limit of approximately 3 A, so no saturation was observed. Its interval type-2 fuzzy reaching action should therefore be understood as trading smoother actuation for stronger disturbance rejection, rather than as a chattering-reduction technique.

Overall, the proposed controllers offer complementary advantages. The IT2FL controller is more appropriate when smooth actuation, reduced control effort, and accurate reference tracking are prioritized, whereas the IT2FL-SMC controller is preferable when robustness and disturbance rejection are the main objectives. Further improvement of the IT2FL-SMC tracking response could be achieved through independent tuning of its fuzzy scaling gains and sliding-surface parameters.

Author Contributions: S.N.: Conceptualization, methodology, software, validation, formal analysis. L.M.: Conceptualization, formal analysis, writing—review and editing, supervision. D.P.-E.: Writing—original draft, review and editing. All authors have read and agreed to the published version of the manuscript.

Funding: This research received no external funding.

Institutional Review Board Statement: Not applicable.

Informed Consent Statement: Not applicable.

Data Availability Statement: The data presented in this study are available on request from the corresponding author.

Conflicts of Interest: The authors declare no conflicts of interest.

Abbreviations

The following abbreviations are used in this manuscript:

FOU	Footprint of uncertainty
FOPDT	First-order-plus-dead-time
IAE	Integral of the absolute error
ISE	Integral of the squared error
IT2FL	Interval Type-2 fuzzy logic controller
IT2FL-SMC	Interval Type-2 fuzzy logic sliding-mode controller
LMF	Lower membership function
MISO	Multiple-input/single-output
PID	Proportional–integral–derivative
SMC	Sliding-mode control
TVU	Total variation of the control input
UAV	Unmanned aerial vehicle

UMF	Upper membership function
VTOL	Vertical takeoff and landing

References

1. Floreano, D.; Wood, R.J. Science, technology and the future of small autonomous drones. *Nature* **2015**, *521*, 460–466. [CrossRef]
2. Misra, A.; Jayachandran, S.; Kenche, S.; Katoch, A.; Suresh, A.; Gundabattini, E.; Selvaraj, S.K.; Legesse, A.A. A review on vertical take-off and landing (VTOL) tilt-rotor and tilt wing unmanned aerial vehicles (UAVs). *J. Eng.* **2022**, *2022*, 1803638. [CrossRef]
3. Ilyas, M.; Khan, M.A.; Arshad, A.; Shahzad, M. Altitude stabilization of VTOL system with nonlinear control strategy. *IEEE Access* **2025**, *13*, 41300–41308. [CrossRef]
4. Hassani, H.; Mansouri, A.; Ahaitouf, A. Performance evaluation of control strategies for autonomous quadrotors: A review. *Complexity* **2024**, *2024*, 8820378. [CrossRef]
5. Aguas, X.; Revelo, J.; Paredes, I.; Cuaycal, A.; Herrera, M. Integral-optimal sliding mode control for vertical take-off and landing system. In Proceedings of the 2018 International Conference on Information Systems and Computer Science (INCISCOS), Quito, Ecuador, 13–15 November 2018; pp. 29–35.
6. Herrera, M.; Leica, P.; Chávez, D.; Camacho, O. A blended sliding mode control with linear quadratic integral control based on reduced order model for a VTOL system. In Proceedings of the 14th International Conference on Informatics in Control, Automation and Robotics (ICINCO), Madrid, Spain, 26–28 July 2017; Volume 1, pp. 606–612.
7. Jacob, J.; Selva Kumar, S. Sliding mode control of VTOL system. *IOP Conf. Ser. Mater. Sci. Eng.* **2019**, *561*, 012069. [CrossRef]
8. Rendón, J.E.; Mejía, C.E. Fractional order modeling of a nonlinear electromechanical system. *Enfoque UTE* **2018**, *9*, 45–56. [CrossRef]
9. Utkin, V.I. Variable structure systems with sliding modes. *IEEE Trans. Autom. Control* **1977**, *22*, 212–222. [CrossRef]
10. Camacho, O.; Smith, C.A. Sliding mode control: An approach to regulate nonlinear chemical processes. *ISA Trans.* **2000**, *39*, 161–177. [CrossRef]
11. Zhao, Q.; Jia, F.; Shao, H. Chattering reduction of sliding mode control for quadrotor UAVs based on reinforcement learning. *Drones* **2023**, *7*, 420. [CrossRef]
12. Hou, Q.; Wang, H.; Lee, C.H.T.; Ding, S. Composite adaptive super-twisting sliding mode control using barrier function for PM motor drives toward electric aircraft applications. *IEEE Trans. Power Electron.* **2025**, *40*, 16255–16264. [CrossRef]
13. Hou, Q.; Wang, H.; Zhao, C.; Xu, S.; Zuo, Y.; Lee, C.H.T. Super-twisting extended state observer-based quasi-proportional-resonant controller for permanent magnet synchronous motor drive system. *IEEE Trans. Transp. Electrif.* **2023**, *10*, 1596–1604. [CrossRef]
14. Zadeh, L.A. Fuzzy sets. *Inf. Control* **1965**, *8*, 338–353. [CrossRef]
15. Hagras, H. A Type-2 fuzzy logic controller for autonomous mobile robots. In Proceedings of the 2004 IEEE International Conference on Fuzzy Systems, Budapest, Hungary, 25–29 July 2004; Volume 2, pp. 965–970.
16. Mendel, J.M.; John, R.I.; Liu, F. Interval Type-2 fuzzy logic systems made simple. *IEEE Trans. Fuzzy Syst.* **2006**, *14*, 808–821. [CrossRef]
17. Nishanth, F.P.; Dash, S.K.; Mahapatro, S.R. Critical study of Type-2 fuzzy logic control from theory to applications: A state-of-the-art comprehensive survey. *e-Prime—Adv. Electr. Eng. Electron. Energy* **2024**, *10*, 100771. [CrossRef]
18. Karnik, N.N.; Mendel, J.M. Centroid of a Type-2 fuzzy set. *Inf. Sci.* **2001**, *132*, 195–220. [CrossRef]
19. Sarabakha, A.; Fu, C.; Kayacan, E.; Kumbasar, T. Type-2 fuzzy logic controllers made even simpler: From design to deployment for UAVs. *IEEE Trans. Ind. Electron.* **2018**, *65*, 5069–5077. [CrossRef]
20. Zeghlache, S.; Benslimane, T.; Amardjia, N.; Bouguerra, A. Interval Type-2 fuzzy sliding mode controller based on nonlinear observer for a 3-DOF helicopter with uncertainties. *Int. J. Fuzzy Syst.* **2017**, *19*, 1444–1463. [CrossRef]
21. Zeghlache, S.; Benslimane, T.; Bouguerra, A. Active fault tolerant control based on interval Type-2 fuzzy sliding mode controller and nonlinear adaptive observer for 3-DOF laboratory helicopter. *ISA Trans.* **2017**, *71*, 280–303. [CrossRef]
22. Sabzalian, M.H.; Zhakiyev, N.; Yedilkhan, D.; Mohammadzadeh, A. An intelligent control strategy for UAVs using adaptive Type-3 fuzzy logic with real-time uncertainty bounds and parallel auxiliary compensation. *Results Control Optim.* **2026**, *23*, 100690. [CrossRef]
23. Quanser Inc. *QNET VTOL—Workbook (Instructor)*; Quanser Inc.: Markham, ON, Canada, 2011.
24. Mendel, J.M. *Uncertain Rule-Based Fuzzy Systems: Introduction and New Directions*; Springer: Cham, Switzerland, 2017.
25. Mendel, J.M.; Hagras, H.; Tan, W.W.; Melek, W.W.; Ying, H. *Introduction to Type-2 Fuzzy Logic Control: Theory and Applications*, 1st ed.; John Wiley & Sons/IEEE Press: Hoboken, NJ, USA, 2014.
26. Nie, M.; Tan, W.W. Towards an efficient Type-reduction method for interval Type-2 fuzzy logic systems. In Proceedings of the 2008 IEEE International Conference on Fuzzy Systems, Hong Kong, China, 1–6 June 2008; pp. 1425–1432.

27. Camacho, C.; Alvarez, H.; Espin, J.; Camacho, O. An internal model based–sliding mode control for open-loop unstable chemical processes with time delay. *ChemEngineering* **2023**, *7*, 53. [CrossRef]
28. Shuaib, A.O.; Ahmed, M.M. Robust PID control system design using ITAE performance index (DC motor model). *Int. J. Innov. Res. Sci. Eng. Technol.* **2014**, *3*, 15060–15067. [CrossRef]

Disclaimer/Publisher's Note: The statements, opinions and data contained in all publications are solely those of the individual author(s) and contributor(s) and not of MDPI and/or the editor(s). MDPI and/or the editor(s) disclaim responsibility for any injury to people or property resulting from any ideas, methods, instructions or products referred to in the content.